SANDIA REPORT

SAND2006-7002
Unlimited Release
Printed November 2006

Nanotube Cathodes

Paul A. Miller, Michael P. Siegal, Donald L. Overmyer, and Thomas R. Lockner

Approved for public release; further dissemination unlimited.

Sandia National Laboratories

Nanotube Cathodes

Paul A. Miller, Michael P. Siegal, Donald L. Overmyer, and Thomas R. Lockner

Sandia National Laboratories
P. O. Box 5800
Albuquerque NM 87185-1423

Summary

Carbon nanotubes have shown promise for applications in many diverse areas of technology. In this report we describe our efforts to develop high-current cathodes from a variety of nanotubes deposited under a variety of conditions. Our goal was to develop a one-inch-diameter cathode capable of emitting 10 amperes of electron current for one second with an applied potential of 50 kV. This combination of current and pulse duration significantly exceeds previously reported nanotube-cathode performance. This project was planned for two years duration. In the first year, we tested the electron-emission characteristics of nanotube arrays fabricated under a variety of conditions. In the second year, we planned to select the best processing conditions, to fabricate larger cathode samples, and to test them on a high-power relativistic electron beam generator.

In the first year, much effort was made to control nanotube arrays in terms of nanotube diameter and average spacing apart. When the project began, we believed that nanotubes approximately 10 nm in diameter would yield sufficient electron emission properties, based on the work of others in the field. Therefore, much of our focus was placed on measured field emission from such nanotubes grown on a variety of metallized surfaces and with varying average spacing between individual nanotubes. We easily reproduced the field emission properties typically measured by others from multi-wall carbon nanotube arrays.

Interestingly, we did this without having the helpful vertical alignment to enhance emission; our nanotubes were randomly oriented. The good emission was most likely possible due to the improved crystallinity, and therefore, electrical conductivity, of our nanotubes compared to those in the literature. However, toward the end of the project, we learned that while these 10-nm-diameter CNTs had superior crystalline structure to the work of others studying field emission from multi-wall CNT arrays, these nanotubes still had a thin coating of glassy carbon surrounding them in a sheath-like

manner. This glassy carbon, or nano-crystalline graphite, is likely to be a poor conductor due to phonon scattering, and should actually be deleterious for extracting electrons with electric fields.

While we did not achieve the field emission reported for single-wall carbon nanotubes that spurred the idea for this project, at the year's very end, we had a breakthrough in materials growth and learned to control the growth of very-small diameter nanotubes ranging from 1.4 to 7 nm. The 1.4-nm nanotubes are single-walled and grow at only 530 ˚C. This is the lowest temperature known to result in single-wall carbon nanotubes, and may be very important for many applications that where certain substrates could not be used due to the high temperatures commonly used for CNT growth. Critically important for field emission, these small diameter nanotubes, consisting of only a few concentric graphene cylindrical walls, do not show the presence of a poorly-conductive sheath material. Therefore, these nanotubes will almost definitely have superior field emission properties to those we already measured, and it is possible that they could provide the necessary field emission to make this project successful. Controlled spacing and lengths of these single-wall nanotubes have yet to be explored, along with correlating their structures to their improved field emission.

Unfortunately, we did not discover the methods to grow these highly-crystalline and small diameter CNTs until late in the year. Since we did not achieve the necessary emission properties by mid-year, the project was 'prematurely' terminated prior to the start of the second year. However, it should be noted that with the late developments, this work has not hit the proverbial 'brick wall.' Clearly the potential still exists to reproduce and even exceed the high emission results reported for randomly-oriented and curly single-wall carbon nanotubes, both in terms of total field emitting currents and perhaps more importantly, in reproducibility.

Acknowledgements

Intentionally left blank.

Contents

Figures

Intentionally left blank.

Nanotube Cathodes

1 Introduction

Carbon nanotubes (CNTs) are of interest for a wide variety of applications. In this report we describe our attempts to develop a field emission source for use in a long-pulse, high-power relativistic electron beam source. Much previous work investigated electron-emission properties of nanotubes for use in diverse applications such as display panels, microwave tubes, x-ray tubes, vacuum microelectronics, and electron-beam accelerators. Descriptions of such efforts are available in book form.[1]

The most prominent past work in developing nanotube cathodes for electron-beam generators was performed by Shiffler et al.[2] They reported using a nanotube cathode in a pulser operating repetitively at 3 Hz, ~300 kV, ~3 kA (~50 A/cm^2) for several thousand shots. Whereas their work involved relatively short pulses (~1 μs), our goal was to develop a cathode capable of emitting 10 A for 1 second from a 1-inch-diameter cathode (2 A/cm^2) with 50 kV applied potential. Our desired level of performance significantly exceeds published results for long-pulse tests.

There were two parts to our project. The first part included fabrication by chemical vapor deposition of arrays of carbon nanotubes and testing the emission of those arrays in a small test bed. In this work we developed and tested a variety of fabrication techniques. That part of the project was scheduled for the first year. The second part (second year) of the project was fabricating larger-area nanotube-array cathodes and testing those cathodes using an intense electron beam pulser. The project was terminated before we could demonstrate arrays that were clearly better than the existing state of the art in the first year of our work. In this report we describe the results of the first part of the project.

2 Metrics

Desirable cathode properties include high-current emission at low applied electric field along with longevity and ruggedness. In addition, we want to avoid current-saturation phenomena, except that imposed by the space charge limit (Child's law). Electron emission occurs by field emission described by the Fowler-Nordheim formula[1]

$$I = aV^2 \exp\left(-b\phi^{3/2}/\beta V\right). \tag{2.1}$$

Most workers measure an emission threshold stated in terms of the minimum electric field at which significant electron current flows. This is somewhat subjective because it depends on the sensitivity of the current measurement system. In published measurements, people often report measuring threshold electric fields of a few volts per micrometer for currents in the microampere range[3]. In other work[4], current measurements extend to the pico-ampere level, which results in lower reported threshold electric fields. Note that Eq. 2.1 is continuous with no specific threshold.

For our application to long-pulse electron beam generation, work reported by Gao et al.[5] and by Yue et. al.[6] is relevant. They report quasi-steady-state currents of tens of milli-amperes from nanotube arrays with several square millimeter areas. Specifically, Gao et al.[5] obtained 4 mA from a 6-mm^2 array (67 mA/cm^2) at 10 V/µm (100 kV/cm) for many hours using 1-s pulses at one minute repetition rate. Yue et al.[6] observed threshold emission of 1 mA/cm^2 at 2 V/µm, and 2-ms current pulses (10% duty cycle) of 145 mA/cm^2 at 6 V/µm.

For our work to be totally successful from an application viewpoint, we wanted to obtain substantially higher emission currents at lower fields than the values cited above, such as 2 A/cm^2 at < 2 V/µm. The main reason for entertaining the possibility of success by this metric is that we fabricate nanotube arrays using different techniques and with different characteristics than tested in any prior work.

3 Nanotube fabrication procedures and structures

Many cathode materials have been studied in pulsed-power systems for decades. Field emission and explosive emission are controlled by very small protruberances ("whiskers") on the cathode surface. In passive cathodes, materials such as graphite and velvet (cloth, carbon) are used with success. Our ability to fabricate arrays of vertically-aligned CNTs with controlled diameters and spacing is the ideal limiting case of exercising precise control over a whisker array. CNTs have the best field-emission properties known with the lowest turn-on fields and the highest current densities. Furthermore, we have some degree of control over CNT resistance via control of diameter. Low resistance is desirable for field-emitting cathodes; higher resistance might be optimum for explosive emission because of the control over I^2R heating rates.

Most studies focus on single-wall CNTs, consisting of a single-graphene-layer cylinder. Such materials grow at high temperature, are difficult to manipulate into useful geometries, and are often semiconducting. Zhu et al made large-current field-emitter films by drying single-wall CNT-containing liquids onto Si.[3] The resulting morphology (left photo in Figure 1) looks like a plate of spaghetti, limiting the lifetime, uniformity, and perveance of the cathode. Conversely, multi-wall CNTs consist of several graphene sheets rolled into concentric cylinders. They grow at lower temperatures directly onto substrates in useful configurations and always are conducting. Siegal co-authored the first reports of CNT arrays on glass and Si substrates, shown in the middle photo in Figure 1.[7,8] *(Note: With over1000 citations, the Science paper is already the 8th most highly-cited SNL paper.[7])* Following our aligned CNT growth publications, Li et al reported a simpler, thermal CVD method for growing highly aligned CNTs that uses an anodized aluminum-oxide (AAO) nano-pore template for alignment.[9] This method is advantageous since growth occurs in a controlled and intrinsically scaleable tube-furnace, and results in a close-packed hexagonal arrangement of CNTs (right photo in Figure 1).
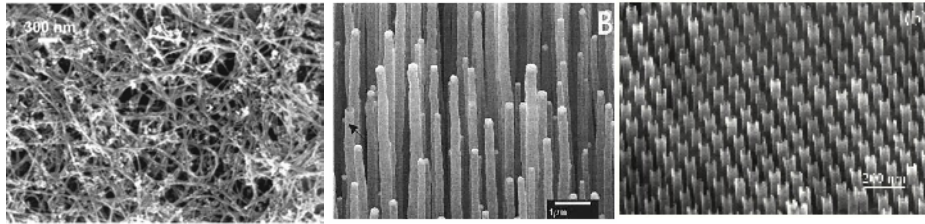
Figure 1. Nanotube sample geometries. Left: non-aligned CNTs from ref. 3 that achieved 4 A/cm^2 field-emission current density. Middle: highly aligned CNT "forest" grown using hot-filament, plasma-enhanced CVD without the use of a template[7]. Right: ordered CNT array by Li et al. grown using an AAO-ordered array template of nanoholes[9].

To achieve high field-emitting current densities along with good lifetime, uniformity, and high perveance (= $I/V^{3/2}$), several CNT structural properties must be improved: crystallinity, average spacing, and alignment. Note that fabricated arrays have large CNT outer diameters, typically ranging from 25 – 500 nm with poor crystallinity. This is obvious in the middle photo in Figure 1, which shows both nonuniform diameters along individual CNT lengths and wide diameter ranges within a sample, leading to poor conductivity and field emission control and reproducibility. CNTs with diameters ≤ 7 nm are highly-crystalline and are likely good conductors, while larger diameter CNTs have an amorphous-to-glassy carbon sheath around a core CNT with significant phonon scattering leading to poor conductivity and field-emission. Also, the near proximity of adjacent CNTs causes self-shielding, effectively limiting field emission. Electron-beam lithography experiments find that self-screening minimizes with average CNT spacing of a few microns.[10] We recently demonstrated such spacing control via inexpensive growth condition controls, shown in Figure 2.[11] Finally, while CNTs in nearly any configuration field emit, as evidenced by the spaghetti-like morphologies of the left photo in Figure 1, vertical alignment similar to the middle and right photos in Figure 1 promote better emission properties.[12] We intended to use a combination of growth conditions and AAO templates to, for the first time, simultaneously control CNT diameter, spacing and orientation for optimal high-current field-emission and explosive-emission applications. This project was terminated before we could study the use of AAO templates.
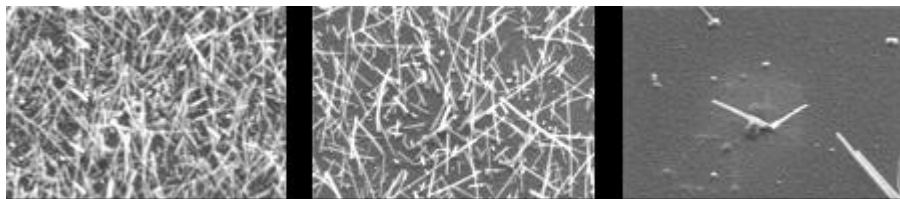
Figure 2. SEMs of 10-nm-diameter CNTs controllably grown to greatly different average spacing, using acetylene, ethylene, and methane as the hydrocarbon feed gases, respectively. The field of view is ~ 1.5 μm^2.

To grow CNTs on Si(100) substrates, we first need to deposit a diffusion barrier to prevent unwanted silicidation between the substrate and the metal catalyst, which occurs at temperatures below those used for CNT growth. After cleaning Si(100) with an HF dip, followed by a DI water rinse, wafers are loaded into an RF sputter deposition system. First, a 50-nm-thick W diffusion barrier is deposited, followed by a 2- to 10-nm-thick layer of Ni metal catalyst. While we have learned to deposit W metal with negligible residual stress, the Ni layers always contain a small level of stress. We use this to control the overall stress in the Ni/W layers, which acts as a further control of the nucleation site density of CNTs during the CVD growth, similar to that shown in Figure 2 (using different hydrocarbons with various levels of chemical reactivity).[11] Due to the large differences in thermal expansion coefficients between Si and Ni/W, the metal layers tend to spall from the substrate during the thermal CVD process. Therefore, we deposit the metals through an Al-foil mask consisting ~ 1 mm holes, resulting in small dots of Ni/W metallization. The residual stresses arising from thermal heating are insufficient to cause spallation of such small areas. Our mask consists of 9 dots over a 1-cm^2 area.

We grow multi-wall CNTs by CVD in a tube furnace at atmospheric pressure (~620 Torr in Albuquerque, NM) from a 1:9 mixture of hydrocarbon:N_2 gases. For this work, we primarily used acetylene as the hydrocarbon feed gas. Acetylene has a high heat of formation and a very reactive hydrocarbon, yielding high densities of CNTs on surfaces. We also grew some samples using methane to get greater spacing between the CNTs to limit self-shielding effects during field-emission. Annealing in flowing CO for 1 hour at 600 ˚C chemically reduces the surface of the Ni layer, enabling CNT nucleation to occur. Following this oxide reduction, the tube furnace is flushed with N_2 and the temperature changed to that desired for CNT growth. Once the desired growth temperature is reached, the furnace is flushed with the gas mixture used for the growth ambient. All CNT samples for this study grew in 15 minutes. CNT diameters are controlled directly by growth temperature.[13] For this project, we studied CNTs grown at temperatures ranging from 530 – 650 ˚C. At the end of the prescribed growth period, the furnace is flushed with N_2 and furnace-cools to < 100 ˚C in approximately 1 hour.

Most of the work in this project was performed on nanotubes grown at 650 ˚C under a variety of conditions that were designed to impact the average spacing between the CNTs. Field-emission measurements on such samples, shown in the next section, found that the overall emission properties were similar to those reported in the vast literature on this subject.[14] While such properties are entirely sufficient for the low emission currents required for many applications, such as displays or nano-electrodes for electrochemical sensing, they fall well-short of the needs for pulsed-power applications.

14

High-resolution transmission electron microscopy (TEM) perhaps explains the limitations of CNTs grown at temperatures ≥ 650 ˚C. Samples were prepared for TEM by lightly agitating the CNT films in acetone to remove them from the Si substrate and get them into solution. Drops of such solutions were then deposited onto a holey-carbon TEM grid for analysis. Figure 3 shows images from nanotubes grown at 630 and 650 ˚C. The left photo (the sample grown at the lower temperature) shows nanotube bundles. This is always seen for single-wall CNTs that are suspended in solutions. This image is taken from the edge of such a bundle where the transmission of
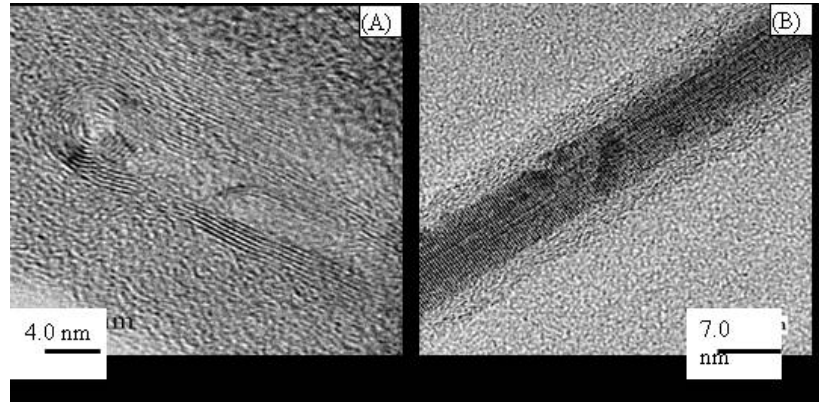
Figure 3. High-resolution TEM images from samples grown at (left) 630 ˚C and (right) 650 ˚C.

electrons through the sample managed to find a single CNT. Clearly, this image demonstrates the presence of a highly-crystalline nanotube with 8 concentric graphene cylinders. The hollow core is easily observed and is measured to be 1.2 ± 0.2 nm. Each graphene cylinder represents 0.38 ± 0.01 nm in thickness, resulting in a total outer diameter of 7.3 nm.

The right photo in Figure 3 shows a CNT grown at 650 ˚C, the temperature used throughout most of the work in this project. This image was taken in a slightly over-focused mode in order to observe the full structure present. The dark contrast region in the middle of the tube represents the crystalline portion of the CNT, with structure and dimensionality similar to that found for the CNT grown at 630 ˚C. However, there also exists an additional feature, present in all nanotubes imaged for growth temperatures ≥ 650 ˚C. This is the lighter contrast region appearing to surround the crystalline part of the nanotube. This region consists of a highly-disordered graphitic material, most likely nano-crystalline graphite, also known as glassy-carbon. Interestingly, TEM sample preparation from samples grown at these elevated temperatures always found isolated nanotubes for imaging, suggesting that glassy-carbon acts as a surfactant for nanotubes and prevents the development of van der Waals' forces that result in their bundling. This glassy-carbon sheath provides the additional diameter to the CNTs observed by SEM. Since glassy-carbon is so highly-disordered, it is not a good electrical conductor. The presence of this sheath material surrounding the nanotubes is expected to negatively impact the field-emission properties, and is perhaps the reason our measurements were not as good as some of the literature reports for single-wall CNTs.

The results shown in Figure 3 clearly suggest that work for this project should focus on the growth of CNTs at temperatures at or below 630 ˚C in order to optimize nanotube conductivity with improved structure and to prevent the formation of what may be a slightly insulating or dielectric sheath layer that most likely has a deleterious affect on field emission. Therefore, toward the end of the project year, we explored low temperature growth for the first time. It should be noted that there is no information in the literature indicating that high-quality carbon nanotubes can be grown at low-temperatures (below 630 ˚C).

We explored CNT growth to as low as 530 ˚C. Figure 4 shows SEM images from samples grown at various low temperatures. All show high density of CNTs present. We will continue to pursue low-temperature growth. There is no fundamental reason that 530 ˚C is a minimum, we simply ran out of time. Note that the spatial resolution of the SEM in use is ~ 10 nm, therefore all the CNTs for these films appear to have the same diameter.
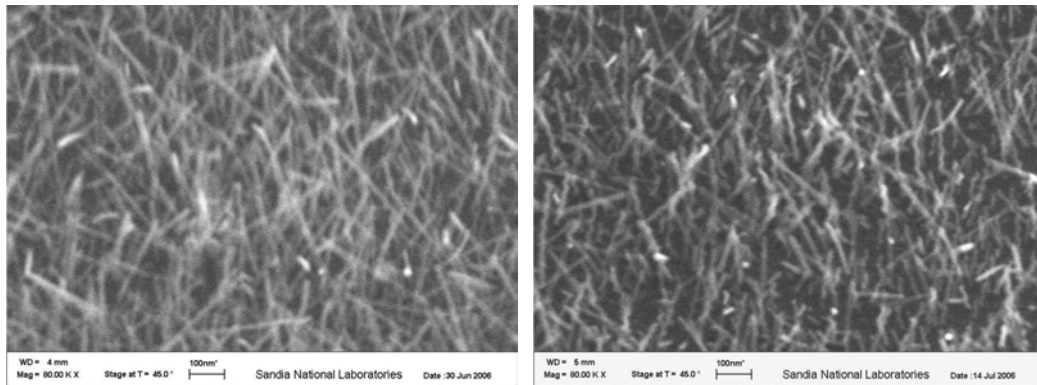
Figure 4. SEM images from CNT samples grown at 530 (left) and 590 ˚C (right). Not shown are similar images for samples grown at 550, 570, and 610 ˚C. For all intents and purposes, each sample looks similar by SEM due to the lack of spatial resolution below 10 nm.

To learn more about the nature of these CNTs grown at low-temperatures, high-resolution TEM was performed on nanotubes harvested from the substrates. Figure 5 shows a image from each sample. First note that every sample consists of bundles of CNTs. These bundles formed when the nanotubes were harvested from their substrates, shown in Figure 4. None of these CNTs appear to have the glassy carbon sheath material, observed by TEM in the samples grown at temperatures ≥ 650 ˚C. Since the glassy carbon sheaths were behaving as a surfactant, nothing prevents these clean CNTs from forming bundles via van der Waal's bonding forces.

The presence of nanotube bundles makes interpretation of these TEM images somewhat more difficult since the electron beam is transmitting through multiple nanotubes, assuming that the bundles are cylindrical in nature. Therefore, similar to the left photo in Figure 3, the best place to observe single nanotubes is on the edge of a bundle. Focusing attention to the bundle edges, it is possible to discern individual

16

nanotubes. Intriguingly, the sample grown at the lowest temperature studied, 530 ˚C, appears to consist primarily of single-wall CNTs. The nanotube on the upper edge of the bundle is highlighted in yellow to guide the eye. This is an exceptionally low growth temperature for single-wall CNTs. Measurements can be taken from this image find the outer diameter of these single-wall CNTs to be ~ 1.4 ± 0.1 nm, with a hollow inner core diameter 0.7 ± 1 nm.

The sample grown at 550 ˚C appears to consist primarily of double-wall CNTs. Again, a DWCNT is highlighted to guide the eye. In all of the samples shown for each growth temperature, the inner core diameter appears to be the same, and that the outer diameters increase by ~ 1 concentric graphene cylinder with every 20 ˚C of increased growth temperature. The average wall thickness of each layer, measured from all of the samples is similar and is 0.375 ± 0.010 nm. This wall thickness compares favorably with the inter-planar spacing existing in graphite of 0.335 nm.
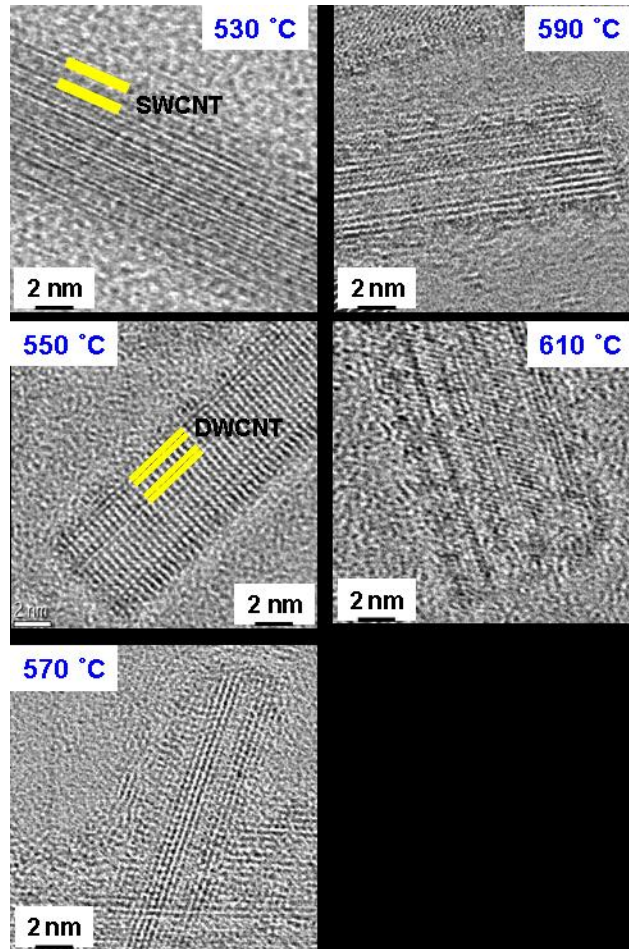
Figure 5. High-resolution TEM images of CNTs harvested from samples at various growth temperatures. These CNTs are all in bundles, held together by van der Waal's forces once removed from the substrate and put into solution.

The outer diameters of the nanotubes observed in Figure 5 can be measured and are plotted in Figure 6. The result shows a linear dependence of CNT outer diameter with increasing growth temperature. Figure 6 also shows the number of graphene concentric cylinders in these CNTs as a function of growth temperature. The linear temperature dependence of both plots shows that CNT diameters increase by adding additional concentric graphene cylinders to the structure. This result differs from that found for CNTs grown at temperatures above 630 ˚C, all of which had a glassy carbon sheath. Therefore, true CNT growth is linear as a function of temperature. It is the growth of glassy carbon that is exponential with temperature, not nanotubes, as previously believed.
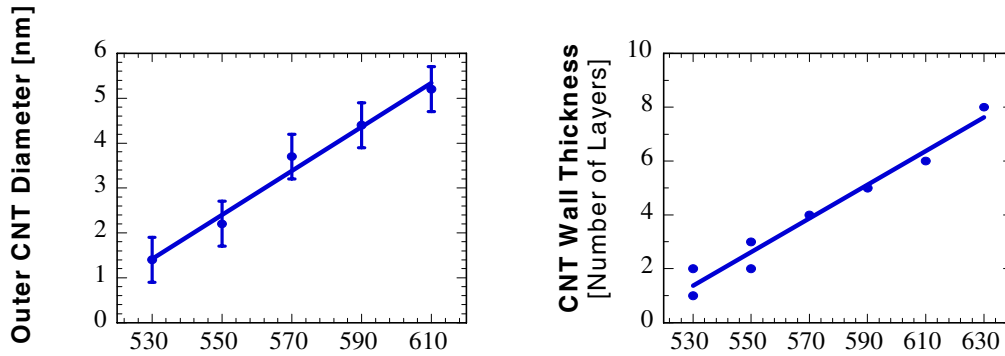
Figure 6. Left: Outer nanotube diameter vs. thermal CVD growth temperature ($^{\circ}$C). Right: CNT wall thickness vs. growth temperature ($^{\circ}$C).

Raman spectroscopy is often used to ascertain the nature of carbon-carbon bonding in nano-crystalline carbon materials due to the resonant enhancement of sp^2-bonded carbon atoms. Figure 7 shows spectra taken using 514 nm incident radiation for nanotube samples at all the growth temperatures studied. These spectra are typical of that for nano-crystalline graphite, also known as glassy carbon, and consist of two well-known features: the G-peak at $\sim$ 1600 cm^{-1}, representative of graphite, and the D-peak at $\sim$ 1350 cm^{-1} which represents disorder in graphene stacking planes. These spectra were normalized to their G-peaks. Recall that the high-resolution TEM does not observe the presence of glassy carbon as part of these nanotube structures. Therefore, glassy carbon may exist on the substrate surface and dominate these spectra. However, it is more likely that the curvature of the graphene walls, to form cylinders, may appear similar to nano-crystalline graphite, and appear to consist of small domains of graphene clusters. Finally, while these spectra are all very similar to one another, note that the spectra for the two lowest temperature samples, those grown at 530 and 550 ˚C, have a slightly smaller D-band than the other samples. Recall that these samples contain primarily single and double-wall CNTs, which perhaps have more crystalline order than larger multi-wall CNTs.

Figure 7. Raman spectra for CNTs on W-coated Si grown at temperatures ranging from 530 to 610 ˚C.

18

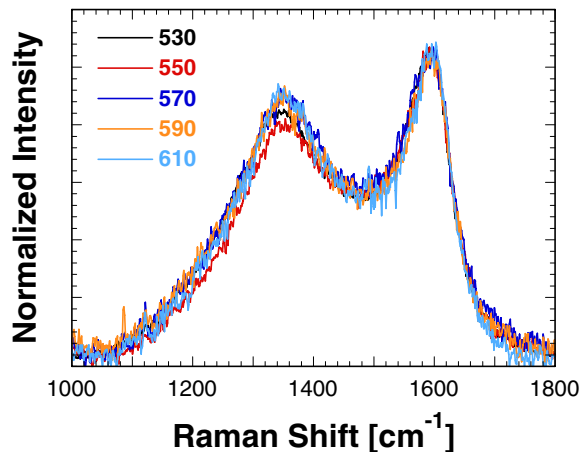Figure 8 compares these low-growth-temperature Raman spectra with those from samples grown at the higher temperatures used to make field emitter samples for most of this project. The sample grown at 610 ˚C is used as the lower temperature limit since it is nearly identical to CNT samples grown as low as 570 ˚C, and therefore can be considered representative of all those samples. Also, CNTs grown at the next elevated temperature, 630 ˚C, are found to consist of nanotubes with significantly larger inner core diameters. Finally, samples grown at even higher temperatures begin to develop glassy carbon sheaths.
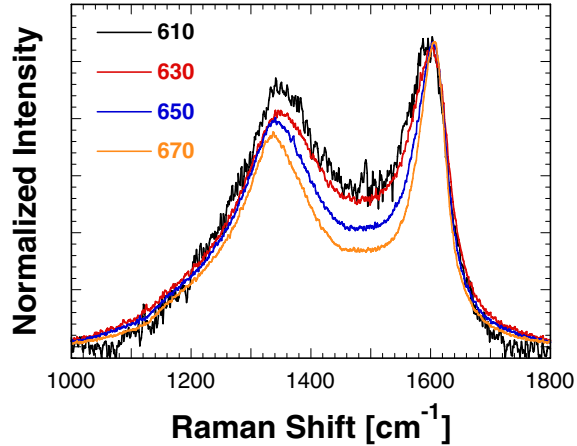

Figure 8. Raman spectra for CNTs on W-coated Si grown at temperatures ranging from 610 to 670 ˚C.

Again, the Raman spectra are normalized to their G-peaks. Observe that the D-peak decreases slightly with increasing growth temperature over this range of samples. Also note the narrowing of both the D- and G-bands with increasing growth temperature. The shrinking of the D-band and the narrowing of both bands is indicative of exposing nano-crystalline graphitic to higher temperatures where the nano-domains are likely growing somewhat in size.

In general, it is fair to state that Raman spectroscopy, while very useful to study subtle changes in amorphous diamond-like carbon, diamond, graphite, glassy carbon, and single wall carbon nanotubes, does not provide the same degree of information when studying multi-wall carbon nanotubes.[15] This has been observed by many groups and is widely reported in the literature. Nevertheless, there have been no reports of such highly crystalline and uniform samples of such small diameter multi-wall CNTs as shown here, and it was hoped that Raman might be more useful.

In summary, we have shown, unfortunately in hindsight, that the CNTs prepared for field emission studies in this project are a composite structure consisting of a highly-crystalline nanotube embedded in a glassy carbon sheath. Due to its high degree of crystalline disorder, this sheath material is expected to be a poor conductor, perhaps even insulating. The existence of such a sheath surrounding a nanotube should have a deleterious effect on field emission properties. Such CNT structures are very similar to those typically reported for field emission measurements, and therefore, we should expect field emission properties similar to that reported by other groups measuring multi-wall CNT arrays. Any future work (not presently planned) should focus on controlling the site density of CNTs formed without the glassy carbon sheath material, as well as preparing vertical alignment of such CNTs using the AAO template method. Such studies have the potential to determine CNT structure – field emission property relationships for the first time due to our unique ability to control such highly crystalline and uniform multi-wall structures.

4 Emission measurement techniques

Nanotube samples were deposited on substrates consisting of silicon wafers that measured approximately 2 cm square. The nanotube samples consisted of arrays of nanotubes arranged as 9 dots, with each dot approximately 2-mm in diameter. The substrates were mounted on a circular stainless-steel back plate and held in place by stainless-steel spring clips that had been spot welded to the back plate. The back plate was attached to an insulated vacuum tube. Figure 9 shows this apparatus. Figure 10 shows a close-up view of the sample in the holder. This test assembly was installed in a vacuum test bed. Typically, tests began with base pressures in the 10^{-8}-Torr range, and the pressure sometimes rose to the 10^{-6}-Torr range during tests.

Figure 9. Vacuum assembly used to support and bias the nanotube arrays deposited on silicon-wafer substrates.

The substrates were biased to negative high potential by a direct-current power supply through a 5-MΩ ballast resistor. An anode consisting of an aluminum or steel pin, somewhat greater than 2-mm in diameter, was mounted in an aluminum block (several cubic centimeters in volume) that served as a heat sink. The anode assembly was supported by an insulated vacuum manipulator assembly that, for most measurements, positioned the anode 0.5 mm away from the nanotube samples. Transverse alignment of the anode was done by two means. Initially, the sample was viewed from the side in reflected light and the anode was positioned by eye over one of the nanotube-array dots. Sometimes, data were taken with this positioning. At other times, a low potential was applied to the nanotube cathode assembly and the anode was scanned transversely to maximize the measured current. The data indicated that positioning by eye was sufficiently accurate for reliable measurements.

Figure 10. Close-up view of sample in holder. Nine nanotube-array dots are visible.

A key metric of cathode performance is electron-emission threshold, but the practical "threshold" is a signal level that depends on the measurement apparatus. The anode assembly in our tests was connected to ground through a 4.7-kΩ current-viewing resistor. For this project, we were most interested in obtaining high emission currents, which led to this choice of relatively low value of resistance. If we had been interested in much lower current levels to detect a very low threshold of emission, we would have used a higher resistance value, as has been used by other workers. The digitizer that we used had a noise level in the sub-millivolt range, which meant that our threshold for current measurement was in the 100-nA range.

The potential applied to the sample and the potential across the current-viewing resistor were measured using a personal computer and data-acquisition board. Typically, 30 measurements were made in rapid succession (~microsecond sampling interval) and averaged to give a single potential-current data point. Such data points were recorded at 0.5- to 1-Hz rate. A data set consisted of a series of such data points that were taken as the power-supply potential was increased in 1-kV steps, from 0 V to 12 kV or more and back to 0 V, with 15 to 30 seconds of data recording at each potential level. The actual potential across the anode-cathode gap differed from the power supply potential because of the ballast and current-viewing resistors.

5 Emission measurements

In this section, we present a sample of emission measurements performed on several nanotube samples. For the most part, the data have been arranged in a common format to facilitate direct comparison of the performance of different samples. However, the reader should be aware that, in some cases, axis scaling varies for clarity.

Figure 11 shows data measured from sample N-12-06-05-1B. The left two graphs show current as a function of applied electric field; the top graph has current plotted linearly and the bottom graph logarithmically. For our 2-mm-diameter emission area, a total current of 1 mA corresponds to current density of 32 mA/cm^2. This sample was the best-performing sample of all tested in this project. If we define the threshold electric field for current flow to be the field required for current in the 1-μA range, then the threshold was approximately 5 V/μm for this sample. The middle two graphs show current as a function of time. In this case, the power-supply potential was increased in 1-kV steps to a maximum of 13 kV, with 30 seconds at each step (60 s at 13 kV), and then reduced back to 0 V at the same rate. The right graph is a plot of the data in a format that facilitates comparison to behavior expected for Fowler-Nordheim emission. For this sample, there was no sign of saturation of emission at the highest current tested.
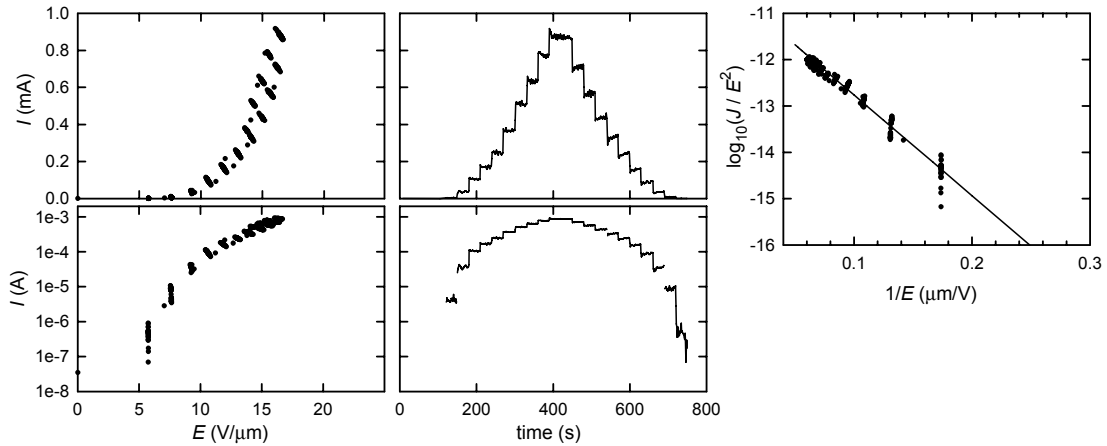
Figure 11. Current vs. potential for sample N-12-06-05-1B. A current of 1 mA corresponds to current density of 32 mA/cm^2. The right-hand graph is a "Fowler-Nordheim" plot. The straight line is a theoretical fit generated using a = 8e-17 and $b\phi^{3/2}/\beta$ = 5e7 (SI units), along with the anode-cathode gap of 0.5 mm.

The straight line in the right graph is a fit generated using the parameters indicated in the caption. In the following graphs, that same line will be presented with those same parameters. It will serve as a simple basis for comparison of sample performance. Figure 12 is data from a repeat test of this same sample, taken 30 minutes after the first test. This shows a measure of the reproducibility obtained in these tests. The second test showed a small amount of hysteresis, with the emission threshold being slightly lower during the latter part of the test when the applied potential was being reduced. The hysteresis might be termed a "conditioning" effect.
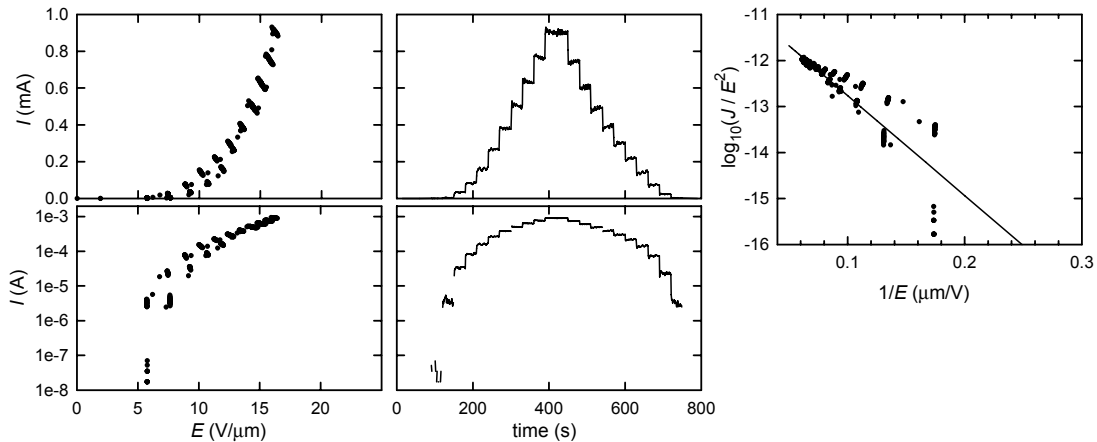

Figure 12. Data from a second test of the same sample shown in Figure 11. Some hysteresis in the characteristics is evident in the left graphs, with a large spread resulting in the Fowler-Nordheim plot.

A frequent occurrence in testing samples was the appearance of visible incandescent hot spots on the silicon wafer. These spots appeared as the potential on the anode was increased. They were associated with increasing current that terminated abruptly along with the disappearance of the hot spots. This led to an emission threshold that increased in time, and corresponding hysteresis. We infer that the hot spots were associated with one or a few nanotubes that "stood tall" on the wafer, glowed due to ohmic heating, and burned up when the current became too large and they got too hot. If the occurrence of these exceptional nanotubes could be controlled and organized into arrays, we would have an excellent cathode.

In contrast to the best sample data, results from sample N-05-09-06-1A, one of the worst samples, are shown in Figure 13 and Figure 14, for which cases the dwell time at each potential was 15 seconds. The former shows emission measured with the anode positioned over one of the cathode dots, and the latter shows emission measured over the uncoated silicon region. The uncoated silicon region, which emitted a blue glow during emission, clearly was a better emitter than this particular formulation of nanotubes, and it displayed minimal hysteresis. For this sample, subsequent analysis by secondary-electron microscope (SEM) showed that there actually were few, if any, nanotubes present. Consequently, poor performance is not surprising. We do not understand the emission mechanism responsible for the results in Figure 14 nor for the blue glow.
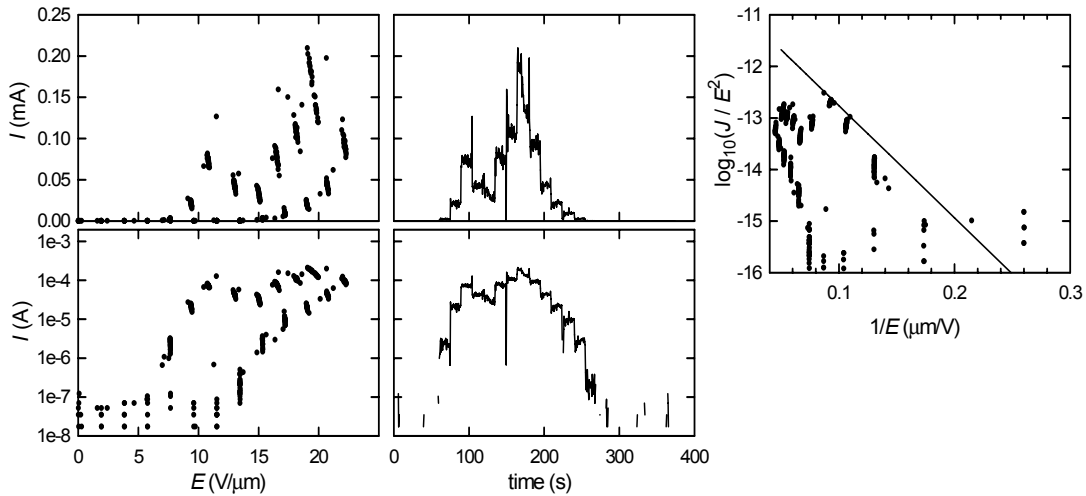

Figure 13. Data from sample N-05-09-06-1A. Note the more-sensitive current scales, which show that this sample was erratic and provided weaker emission than that shown in Figure 11 and Figure 12.
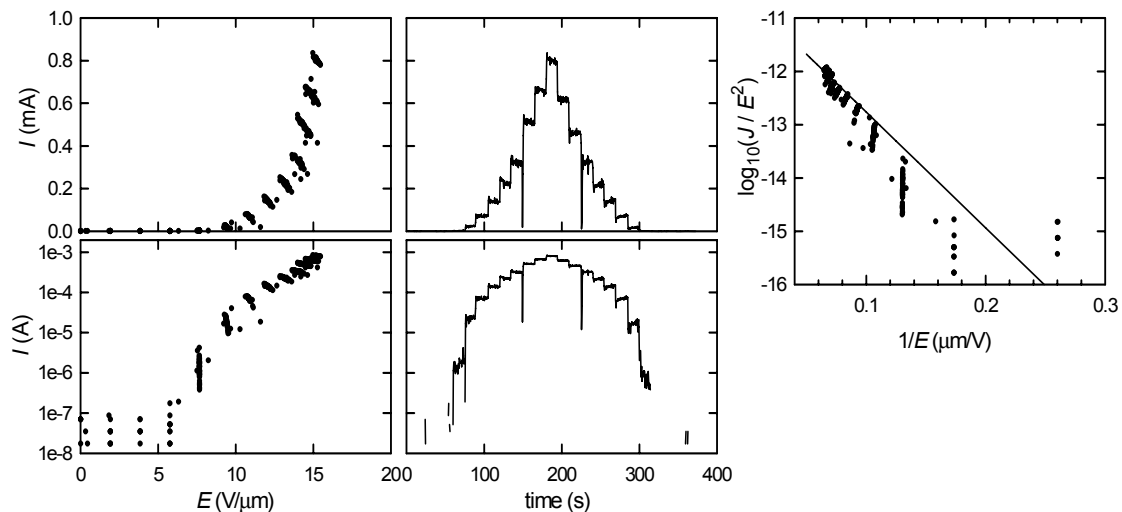
Figure 14. Data from sample N-05-09-06-1A taken with the anode positioned over uncoated silicon away from the nanotube arrays. Emission from the uncoated silicon was superior to that from the nanotube dot and was accompanied by a visible blue glow on the sample.

The data shown in Figure 15 from sample N-05-05-06-1A indicate almost no emission. Emission measured away from the nanotube dots was similar to that shown in Figure 14.

Figure 15.   Data from sample N-05-05-06-1A. This sample clearly was a poor emitter (note the expanded current scale).

Figure 16 shows data from samples N-05-08-06-1A, another poor emitter displaying strong hysteresis. In this case, as was usually the case, emission was better in the first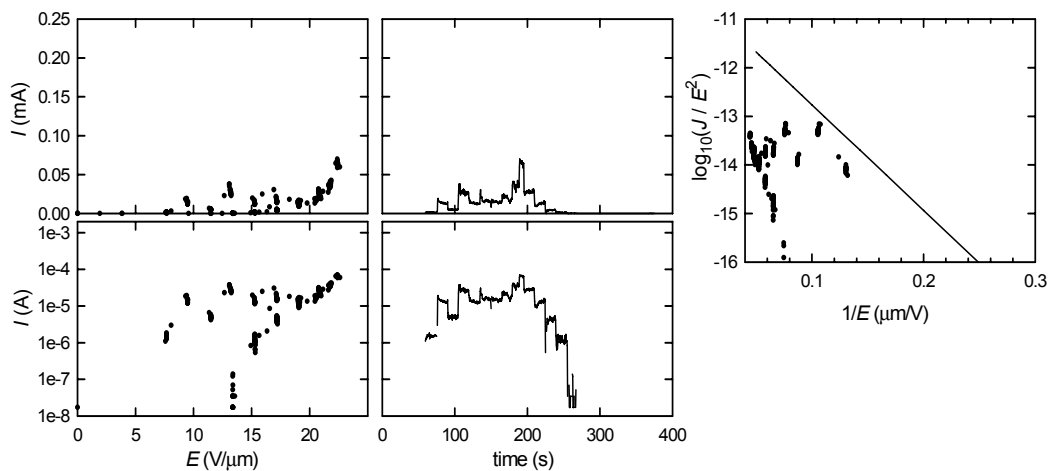 part of the test when the applied potential was being increased. As is shown in the logarithmic current plot, the initial threshold for emission for this sample was quite low.
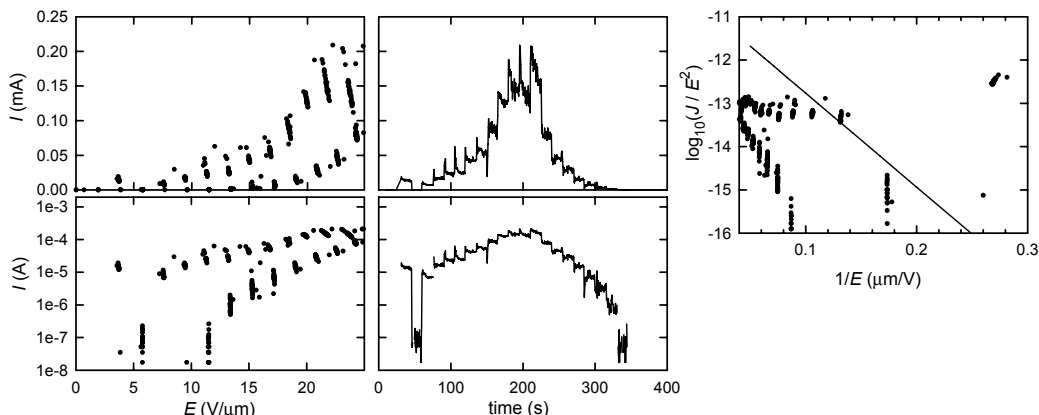

Figure 16. Data from sample N-05-08-06-1A.

6 Conclusions

Electron emission from nanotubes depends on several factors, including the height, diameter, and spacing between nanotubes. Within the range of parameters that we fabricated, our best results (Figure 11 and Figure 12) were comparable to results obtained by other workers. We failed to obtain the vastly superior results that were our goal.

In the first year, much effort was made to control nanotube arrays in terms of nanotube diameter and average spacing. When the project began, we believed that nanotubes approximately 10 nm in diameter would yield sufficient electron emission properties, based on the work of others in the field. Therefore, much of our focus was placed on measured field emission from such nanotubes grown on a variety of metallized surfaces and with varying average spacing between individual nanotubes. We easily reproduced the field emission properties typically measured by others from multi-wall carbon nanotube arrays.

Interestingly, we did this without having the helpful vertical alignment; our nanotubes were randomly oriented. The good emission was most likely possible due to the improved crystallinity, and therefore, electrical conductivity, of our nanotubes compared to those in the literature. However, toward the end of the project, we learned that while these 10-nm-diameter CNTs had superior crystalline structure to the work of

others studying field emission from multi-wall CNT arrays, these nanotubes still had a thin coating of glassy carbon surrounding them in a sheath-like manner. This glassy carbon, or nano-crystalline graphite, is likely to be a poor conductor due to phonon scattering, and should actually be deleterious for extracting electrons with electric fields.

While we did not achieve the field emission reported for single-wall carbon nanotubes that spurred the idea for this project, at the year's very end, we had a breakthrough in materials growth and learned to control the growth of very-small diameter nanotubes ranging from 1.4 to 7 nm. The 1.4 nm nanotubes are single-walled and grow at only 530 ˚C. This is the lowest temperature known to result in single-wall carbon nanotubes, and may be very important for many applications that where certain substrates could not be used due to the high temperatures commonly used for CNT growth. Critically important for field emission, these small diameter nanotubes, consisting of only a few concentric graphene cylindrical walls, do not show the presence of a poorly-conductive sheath material. Therefore, these nanotubes will almost definitely have superior field emission properties to those we already measured, and it is possible that they could provide the necessary field emission to make this project successful. Controlled spacing and lengths of these single-wall nanotubes have yet to be explored, along with correlating their structures to their improved field emission.

Unfortunately, we did not discover the methods to grow these highly-crystalline and small diameter CNTs until late in the year. Since we did not achieve the necessary emission properties by mid-year, the project was 'prematurely' terminated prior to the start of the second year. However, it should be noted that with the late developments, this work has not hit the proverbial 'brick wall.' Clearly the potential still exists to reproduce and even exceed the high emission results reported for randomly-oriented and curly single-wall carbon nanotubes, both in terms of total field emitting currents and perhaps more importantly, in reproducibility.

26

7 References

[1] See Chapter 8, "Field Emission", in *Carbon Nanotubes*, ed. by M. Meyyappan, CRC Press, Boca Raton (2005).

[2] "A High-Current, Large-Area Carbon Nanotube Cathode", D. Shiffler, O. Zhou, C. Bower, M. LaCour, and K. Golby, IEEE Trans. Plasma Sci. **32**, 2152-2154 (2004).

[3] "Low current density from carbon nanotube field emitters", W. Zhu, C. Bower, O. Zhou, G. Kochanski, and S. Jin, Appl. Phys. Lett. **75**, 873-875 (1999).

[4] "Field emission from carbon nanotubes: perspectives for applications and clues to the emission mechanism", J.-M. Bonard, J.-P. Salvetat, T. Stockli, L. Forro, and A. Chatelain, Appl Phys. A **69**, 245-254 (1999).

[5] "Fabrication and Electron Field Emission Properties of Carbon Nanotube Films by Electrophoretic Deposition", Bo Gao, Guozhen Z. Yue, Qi Qiu, Yuan Cheng, Hideo Shimoda, Les Fleming, and Otto Zhou, Adv. Mater. **13**, 1770-1773 (2001).

[6] "Generation of continuous and pulsed diagnostic imaging x-ray radiation using a carbon-nanotube-based field-emission cathode", G. Z. Yue, Q. Qiu, Bo Gao, Y. Cheng, J. Zhang, H. Shimoda, S Chang, J. P. Lu, and O. Zhou, Appl. Phys. Lett. **81**, 355-357 (2002).

[7] Z. F. Ren, Z. P. Huang, J. W. Xu, J. H. Wang, P. Bush, M. P. Siegal, and P. P. Provencio, Science **282**, 1105 (1998).

[8] Z. P. Huang, J. W. Xu, Z. F. Ren, J. H. Wang, M. P. Siegal, and P. P. Provencio, Appl. Phys. Lett. **73**, 3845 (1998).

[9] J. Li, C. Papadopoulos, J. M. Xu, and M. Moskovits, Appl. Phys. Lett. **75**, 367 (1999).

[10] L. Nilsson, O. Groening, C. Emmenegger, O. Kuettel, E. Schaller, L. Schlapbach, H. Kind, J-M. Bonard, and K. Kern, Appl. Phys. Lett. **76**, 2071 (2000).

[11] M. P. Siegal, D. L. Overmyer, and F. H. Kaatz, Appl. Phys. Lett. **84**, 5156 (2004).

[12] Y. Chen, D. T. Shaw, and L. P. Guo, Appl. Phys. Lett. **76**, 2469 (2000).

[13] M. P. Siegal, D. L. Overmyer, and P. P. Provencio, Appl. Phys. Lett. **80**, 2171 (2002).

[14] F. H. Kaatz, M. P. Siegal, D. L. Overmyer, P. P. Provencio, and J. L. Jackson, Mat. Sci. Eng. C, **23**, 141 (2003).

[15] M. S. Dresselhaus, G. Dresselhaus, r. Saito, and A. Jorio, Physics Reports, **409**, 47 (2005).

Distribution

2	MS9018	Central Technical Files, 8944
2	MS0899	Technical Library, 4536
1	MS0123	D. Chavez, LDRD Office, 1011
1	MS1182	Bob Turman, 15335
5	MS1182	Tom Lockner, 15335
1	MS1423	Greg Hebner, 1128
5	MS1423	Paul Miller, 1128
5	MS1086	Mike Siegal, 1126
1	MS1193	John Maenchen, 1645